Chemical Engineering Science 148 (2016) 170–181

Contents lists available at ScienceDirect

Chemical Engineering Science

journal homepage: www.elsevier.com/locate/ces

Autothermal reverse-flow reactors: Design and comparison of valve-operated and rotary systems

Carlos Daniel Luzi [a,b,*], Osvaldo Miguel Martínez [a,b], Guillermo Fernando Barreto [a,b]

[a] PROIRQ, Departamento de Ingeniería Química, Facultad de Ingeniería, UNLP, La Plata, Argentina
[b] Centro de Investigación y Desarrollo en Ciencias Aplicadas "Dr. J. J. Ronco" (CINDECA) CCT La Plata-CONICET – UNLP, Calle 47 No. 257, CP B1900AJK La Plata, Argentina

HIGHLIGHTS

- Valve-operated and rotary reverse-flow reactors are simulated and compared.
- Five different monolithic structures are considered for performance comparison.
- A design strategy is proposed considering a range of VOC content to be treated.
- The rotary scheme avoids the emission of unreacted VOCs after flow reversal.
- The rotary scheme results substantially more compact than the conventional.

ARTICLE INFO

Article history:
Received 23 December 2015
Received in revised form
11 March 2016
Accepted 23 March 2016
Available online 25 March 2016

Keywords:
Volatile organic compounds
Catalytic combustion
Valve-operated reverse-flow reactor
Rotary reverse-flow reactor

ABSTRACT

The valve-operated reverse-flow catalytic reactor is an efficient system for the treatment of air streams contaminated with small amounts of volatile organic compounds (VOCs). Nonetheless, it has two drawbacks when operated at low cycle periods: the emission of the volume without treatment present in the region close to the reactor input and an unavoidable reduction of the valve lifetime. Upon consideration that the use of shorter cycle periods would enable the design of more compact units, we investigated the option of operating with reverse flow by means of a rotary catalytic reactor. This alternative eliminates the necessity of valves for the flow reversal and enables to allot a small fraction of the total cross section to be fed with clean air and prevent the VOCs that remain close to the reactor input from being discharged to the atmosphere.

The aim of this work is to analyse the treatment of an air stream contaminated with ethanol and ethyl acetate by means of mathematical simulation of reverse-flow operations in both valve-operated and rotary catalytic reactors. To that end, monolithic structures with square channels are assumed for both types of reverse-flow reactors, a design strategy is proposed and the results for both types of reactors are compared. It is concluded that the rotary reverse-flow reactor arises as a better option.

1. Introduction

As the result of increasingly demanding environmental regulations, an interest in technology for the control of air contamination has grown considerably in recent decades. Volatile organic compounds (VOCs) are among the most common air contaminants, with catalytic combustion being the usual technology for their elimination when the levels of VOCs are low – *i.e.*, $\leq 1\%$ – (Kolaczkowski, 2006).

The industrial air streams to be purified are usually at near room temperature and, in practice, the flow rates of the air to be processed are quite high. Furthermore, depending on the nature of the substances to be treated and the catalyst used, the temperature necessary for the catalytic combustion ranges between 200 and 400 °C. The necessity therefore arises to utilize combustion schemes that enable an efficient recovery of the energy of the processed gases to raise the temperature of the input air stream.

Among the possible schemes to realize the energy recovery, the reverse-flow system has been widely studied (*e.g.*, Chen et al., 2011; Marín et al., 2010; Matros and Bunimovich, 1996). The system consists in the operation of a catalytic bed (with either a structured or a granular packing) with periodically inversion of the flow direction of the air stream. By this means, the operation

* Corresponding author at: PROIRQ, Departamento de Ingeniería Química, Facultad de Ingeniería, UNLP, La Plata, Argentina.
E-mail address: carlos_luzi@yahoo.com.ar (C.D. Luzi).

http://dx.doi.org/10.1016/j.ces.2016.03.033
0009-2509/

remains transient though with periodically repeated cycles so as to maintain the central zone of the bed at the temperature required for the VOCs combustion, while the ends operate as preheating sectors (Matros and Bunimovich, 1996). This type of operation becomes particularly attractive when the adiabatic temperature rise is low, a condition that occurs in the treatment of VOCs owing to their low concentration.

In practice, the reversal in the direction of the flow is achieved by a valve (or a set of valves) in the conventional scheme. Though this means is the simplest, the use of valves has two disadvantages when the cycle period is short: first, each time the valves change the direction of the flow, they emit the small fraction of the untreated VOCs that remain in the entrance of the unit into the atmosphere; second, the lifetime of a valve is proportional to the cycle period. Both of these features set a lower limit on the cycle period. The use of short cycle periods, however, would enable the design of more compact units. Indeed, the shorter the cycle period, the higher will be the average temperature of the bed. Thus, the operation with flow reversal by means of a rotary scheme in which the bed turns on an axis, while the input air enters and the product is extracted through the use of segmented fixed heads, arises as an interesting option. This alternative eliminates the necessity of valves for the flow reversal and allows avoiding the emission of VOCs close to the reactor inputs, as will be explained in Section 2.1.

The rotary scheme has been postulated by Kolios et al. (2000), who indicated: "An elegant possibility of operating a regenerative fixed-bed reactor in a continuous mode with integrated purge steps without using valves is to use a Ljungström-type rotating-regenerator design". Such a scheme has been proposed for the process of Chemical Looping Combustion (CLC). In this system, the alternative of employing a monolithic-type structure (Lecomte et al., 2010) or a packed bed of particles has been suggested (Noorman et al., 2010). A model of this type of system has been presented by Zhao et al. (2013). To the best of our knowledge in the literature to date no report exists dealing with a modelling and design procedure of a rotary scheme for the treatment of VOCs in order to determine in a concrete manner the advantages of that scheme over the conventional reverse-flow reactor (CRFR).

Within this context, the objective proposed in this contribution is to apply a model of the rotary reverse-flow reactor (RRFR) to the treatment of VOCs to compare the performance of such scheme against the CRFR. For both systems, we propose a design procedure taking into account the fluctuations that could occur in the input air stream. The elimination of a mixture of ethanol and ethyl acetate in an air stream is employed as a case study. A monolithic structure with square channels is assumed for both types of reverse-flow reactors. Five configurations of the monolith cell have been considered in order to select the most suitable one for each type of reactor.

2. Case-study

Ethyl acetate (EA) and ethanol (Et), employed as solvents in printing processes, are typical VOCs released by the manufacture of packaging. The catalytic incineration over Mn and Cu oxides (Morales et al., 2008) of an air stream containing those compounds has been chosen as the case-study. Table 1 presents the specific characteristics of the stream to be treated. In terms of the maximum adiabatic temperature rise, ΔT_{ad}, the minimum and nominal VOC contents shown in Table 1 correspond to 26.6 and 53.2 °C, respectively. The need to consider a minimum content of VOCs will be discussed in Section 5.

The reaction system has been studied by Campesi et al. (2012b). They proved that ethanol combustion goes through the production of acetaldehyde. The reactions and kinetic expressions involved – identified by indices 1, 2, and 3 for ethyl acetate, ethanol, and acetaldehyde, respectively – are:

Table 1
Characteristics of the VOC-laden air stream.

Mass flow rate [kg s^{-1}]	Pressure [bar]	Temperature [°C]	Minimum composition [ppm V]		Nominal composition [ppm V]	
12.7	1.06	50	EA 307	Et 125	EA 615	Et 250

Table 2
Kinetic parameters.

Preexponential factor [s^{-1}]		Activation energy [J mol^{-1}]		Reference temperature [K] and adsorption constant [m^3 mol^{-1}]	
$k_{1,ref}$	6.62×10^1	E_1	1.48×10^5	T_{ref}	448
$k_{2,ref}$	1.81×10^3	E_2	1.10×10^5	K_1	4.19×10^1
$k_{3,ref}$	1.22×10^1	E_3	1.69×10^5	K_3	6.75×10^1

$$C_4H_8O_2 + 5O_2 \rightarrow 4CO_2 + 4H_2O$$

$$C_2H_6O + 1/2O_2 \rightarrow C_2H_4O + H_2O$$

$$C_2H_4O + 5/2O_2 \rightarrow 2CO_2 + 2H_2O$$

$$r_i = \frac{k_i C_i}{1 + K_1 C_1 + K_3 C_3} \qquad \text{for} \quad i = 1..3 \tag{1}$$

$$k_i = k_{i,ref} \exp\left[-\frac{E_i}{R}\left(\frac{1}{T} - \frac{1}{T_{ref}}\right)\right] \qquad \text{for} \quad i = 1..3 \tag{2}$$

Table 2 summarizes the kinetic parameters (Campesi et al., 2012b), which correspond to intrinsic values, as intra-particles diffusional resistances were accounted for in the analysis of the experimental data.

The catalytic reactors are monolithic structures comprising an inert matrix coated with the catalyst. A 10 μm thick uniform catalytic coating, δ_{cat}, was assumed. For the sizing of the units and their comparison, a set of 5 types of square cells, whose characteristics are shown in Table 3, were considered. The dimensions in Table 3 include the catalytic coating. The first three of them correspond to commercial standards of Corning Incorporated (Boger et al., 2004) with 200, 400, and 600 cells per square inch and wall thicknesses of 12.5, 7.5, and 4.0 thousandths of an inch, respectively. Configurations 4 and 5 are alternative designs to numbers 2 and 3, respectively, with the wall thickness having been modified in such a way that the void fraction is the same as that of configuration number 1. The properties of solid structure are evaluated as those of nonporous cordierite (Gulati, 2006).

Table 3
Cell configurations and relevant geometrical properties.

Nº	$10^{-5}N_{cell}$ [m^{-2}]	$10^4\delta_T$ [m]	ε	a_v [m^{-1}]	$10^3 d_h$ [m]
1	3.1	3.18	0.678	1833	1.48
2	6.2	1.91	0.722	2677	1.08
3	9.3	1.02	0.814	3480	0.94
4	6.2	2.25	0.678	2593	1.05
5	9.3	1.83	0.678	3176	0.85

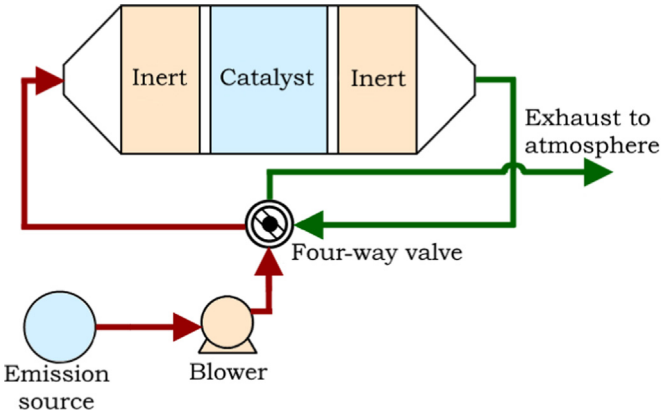

Fig. 1. Simplified scheme of the conventional reverse-flow reactor.

As described in the next section, the ends of the bed are composed of only inert material, but for the calculations they are supposed to keep the same dimensions and properties of the central active zone.

2.1. Description of the reverse-flow schemes

Fig. 1 is a diagram of the conventional reverse flow reactor, CRFR, where the ends of the bed are considered to be made of inert material, since they mainly act as preheating zones (Matros and Bunimovich, 1996). In addition, Fig. 2 provides qualitative temperature and concentration (mole fraction) profiles achieved upon reaching the cyclic steady state (CSS).

As described in the Introduction, short cycle periods in the conventional system are limited by the following two reasons. First, according to Barresi et al. (2007), the valves utilized withstand some 500,000 movements (*i.e.*, 250,000 cycles) during their useful lifetime. Second, as illustrated by the concentration profile shown in Fig. 2, at the end of each semicycle a certain volume of air containing VOCs remains in a significant portion of the bed, which is discharged untreated into the atmosphere once the direction of the air stream is reversed. This undesirable feature is frequently referred to as wash-out problem.

Kolios et al. (2000) described alternatives to avoid the wash-out problem. The use of a rotary reverse-flow reactor (RRFR) enables a suitable solution (Fig. 3). In this scheme, two main compartments can be identified in which the air stream to be treated circulates in opposite directions. The reversal of the flow direction would occur at the moment when a set of channels aligned along the radius of the rotor leave one compartment and enter the other. However, to avoid the wash-out problem, two small compartments should be intercalated (see Fig. 3b). Low flow-rate streams of clean air, diverted from the atmospheric exhausts (Fig. 3), are fed through these secondary compartments to displace the residual VOCs in the channels towards the central zone, where they become incinerated, and replace the frontal zone by a volume of clean air, before the flow reversal.

In this way, two steps are identified for each channel in a semicycle: one is termed “reaction step”, while the channel is connected to a main compartment fed by the waste stream, and the other one, termed “cleaning step”, takes place when the channel is fed by the clean air stream.

As long as the thermal conduction on the angular direction can be neglected, the performance of the RRFR – with the exception of the effect of the cleaning section – is expected to be practically equivalent to that of the CRFR, under the same operating conditions. The practical difference lies in the minimum cycle period allowed by each system. The causes limiting the possibility to operate the CRFR at short cycle periods were already mentioned. On the other hand, the minimum cycle period will be restrained in the RRFR by the feasible rotational speed of the bed. Values between 2 to 10 rpm, as suggested for commercial rotary heat exchangers, will be taken as a reference.

For a given cycle period, t_{cycle}, in the RRFR, the duration of the reaction and cleaning stages, t_R and t_C, will be determined by:

$$t_R = (1 - f_C)\ t_{cycle}/2 \tag{3}$$

$$t_C = f_C\ t_{cycle}/2 \tag{4}$$

where f_C is the fraction of the cross section of the rotor allotted for cleaning (or *cleaning fraction* for short).

3. Modelling

For both alternatives, CRFR and RRFR, a heterogeneous one-dimensional model was employed, without the explicit inclusion of axial dispersion terms. The global mass accumulation in the gas phase, the accumulation of species in the catalyst pores and on the catalyst internal surface, possible homogeneous gas-phase reactions, and energy losses have been neglected. In addition, the inert material was assumed to be non-adsorbent.

It is expected that most of the hypothesis described in the previous paragraph will be satisfied for typical industrial operating conditions. However, due to the dynamic behaviour of the systems, special care must be taken about the effect of accumulation of species on the surface of the catalyst pores. Thus, if certain species strongly cover the catalyst internal surface, accumulation terms for such species should be considered in the model. In addition, if the adsorption-desorption steps for such species are not fast enough, the rates of consumption/production of each compound will be different to that predicted when the catalyst layer is

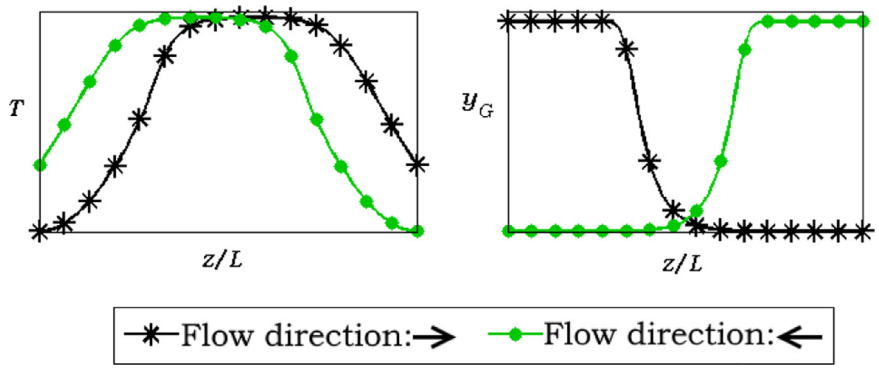

Fig. 2. Typical temperature (left) and composition (right) profiles at the end of two consecutive semicycles at the cyclic steady state (CSS).

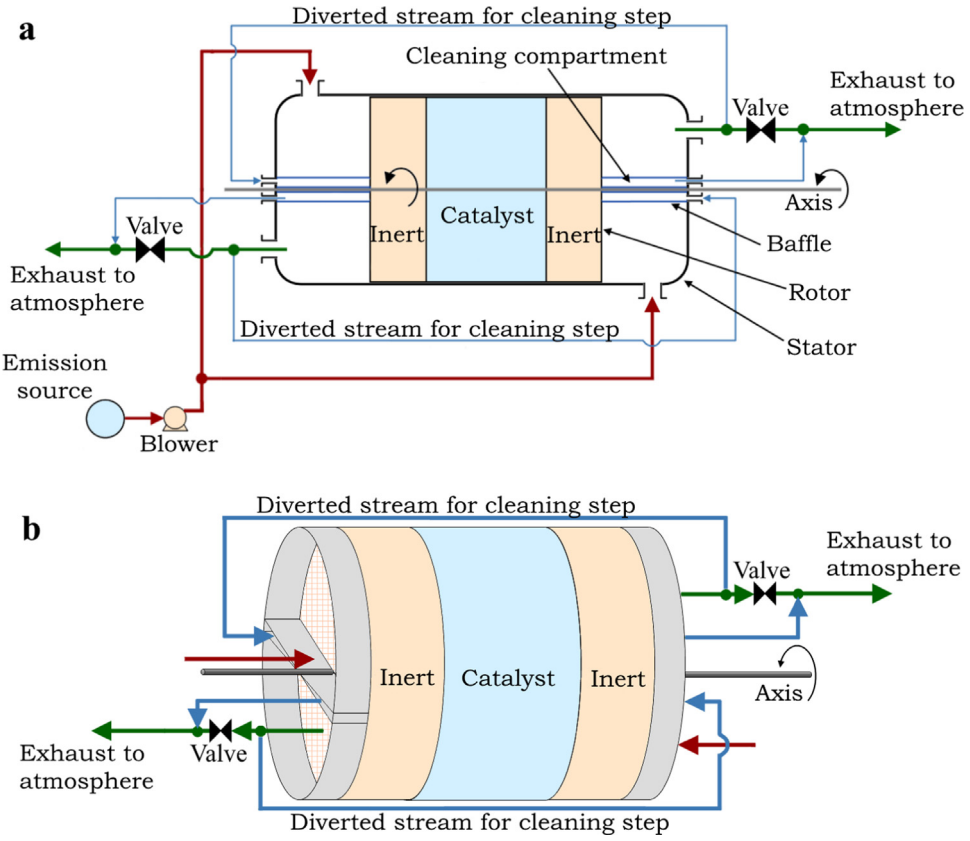

Fig. 3. (a) Scheme of the rotary reverse-flow reactor and (b) detail of the rotor. The valve (▸◂) is actuated to allow the diverted flow into the cleaning step.

considered to be in a (pseudo) steady state. Nonetheless, the analysis and inclusion of such effects are beyond the scope of the present study.

Owing to the low content of VOCs in the air waste stream (below 1%), physical properties of pure air were used. Additionally, ideal gas behaviour for the gas phase was assumed and the variation in the total molar flow rate due to the chemical reactions was considered as negligible.

The pressure drop was calculated by considering that the friction-factor Reynolds number product is equal to 14.2 for square channels. However, the pressure drop along the monolith turned out to be very low as compared to the absolute pressure. Hence, pressure was assumed uniform for solving the energy and mass conservation equations.

The inlet stream was considered to be evenly distributed in the available channels for both systems. For the CRFR, this assumption implies that the behaviour of each channel will be independent of the others, and enables the behaviour of a single channel to be representative of the whole set. For the RRFR, the thermal conduction on the transverse directions was additionally neglected. Under both assumptions, energy and mass balance conservation equations will be the same for any channel of the RRFR.

Accordingly, the following energy and mass balances were applied to simulate the behaviour of both, CRFR and RRFR. For the catalytic zones,

Energy balance in the solid phase:

$$(1-\epsilon)(\rho c_p)_S \frac{\partial T_S}{\partial t} = a_v h^* (T_G - T_S) + a_v \ell \sum_{j=1}^{3} (-\Delta H_j) r_j^{ef} \tag{5}$$

where $\ell = \delta_{cat}[1 + \delta_{cat}/(L_{cell} - \delta_T)]$ is the equivalent washcoat thickness (ratio of the volume of catalytic washcoat to the total transfer area), $L_{cell} = N_{cell}^{-1/2}$ is the side of the unit cell of the monolith, and h^* is a modified heat transfer coefficient, incorporating the effect of axial thermal conduction of the solid materials through an adaptation of the approximation proposed by Vortmeyer and Schaefer (1974),

$$\frac{1}{h^*} = \frac{1}{h} + \frac{a_v \lambda_S}{(G c_{pG})^2} \tag{6}$$

Energy balance in the gas phase:

$$\varepsilon (\rho c_p)_G \frac{\partial T_G}{\partial t} = -G c_{pG} \frac{\partial T_G}{\partial z} - a_v h^* (T_G - T_S) \tag{7}$$

Mass balance for each component in the gas phase:

$$\varepsilon \frac{\partial (C_T\, y_{j,G})}{\partial t} = -\frac{G}{M_{air}} \frac{\partial y_{j,G}}{\partial z} - a_v\, k_{m,j}\, C_T (y_{j,G} - y_{j,S}) \qquad j = 1..3 \tag{8}$$

Mass balance for each component in the solid phase:

$$k_{m,j}\, C_T (y_{j,G} - y_{j,S}) - \ell r_j^{ef} = 0 \qquad j = 1..3 \tag{9}$$

In the end zones, where only inert material is present, the same balances given by Eqs. (5)–(8) apply after dropping the reaction-heat terms in Eq. (5) and the mass transfer term in Eq. (8).

The mass and heat transfer coefficients are calculated from *Sh* and *Nu* numbers at conditions of constant surface concentration/temperature in laminar flow. The asymptotic values for a square channel are $Sh = Nu = 2.977$. However, entrance effects could be significant in laminar flow and, in practice, monolithic structures are assembled by piling modules of predefined length, a feature that repeats those effects. Then, a channel length of 0.25 m was considered and a spatial average value of *Sh* and *Nu* was used, as described by Luzi (2015). The corrected values of *Sh* and *Nu* differed in no more than 5%, and therefore the asymptotic values could have been employed without any practical consequence.

The effective reaction rate for each component is calculated from the approximation proposed by Campesi et al. (2012a), by employing the effective diffusivities reported in that work and the equivalent washcoat thickness ℓ.

3.1. Boundary and initial conditions for the CRFR and solution for the CSS

The solution of the conservation equations presented in Section 3 is intended in this work for evaluating temperature and concentration variations in the CSS. To this end, the actual feeding conditions are established and some arbitrary initial conditions are chosen for a single channel that, as explained before, will represent the whole set, provided the initial conditions are the same for all channels. The transient behaviour is then evaluated until concentration and temperature variations during a cycle remain virtually unchanged in the next cycle. Initial conditions were chosen as $y_{j,G}(0,z)=0$ (clean air), $T_S(0,z)=T_G(0,z)=T^{ini}$, where the value $T^{ini}=350$ °C always allowed to reach, when feasible, the ignited CSS. It is convenient to note that at the end of a semicycle, when the flow is reversed, the new semicycle starts with the same values of temperatures and concentrations. In practice, to keep on working with positive values of the mass velocity G in Eqs. (5)–(8), the coordinate z is reversed. That is, defining $X^{(n)}$ as any of the variables T_S, T_G or $y_{j,G}$ for the nth semicycle ($n \geq 2$):

$$X_{ini}^{(n)}(z) = X_{end}^{(n-1)}(L-z), \tag{10}$$

where $X_{ini}^{(n)}$ is the value of X at the beginning of the current semicycle and $X_{end}^{(n-1)}$ is the value of X at the end of the previous semicycle.

With respect to the boundary conditions, for $z=0$ these are determined by the feed conditions T_G^0 and $y_{j,G}^0$ (see Table 1). On consideration of the model proposed, at the boundary between the inert and catalytic zones, the values of temperature and mole fraction in the gas phase are required to be continuous.

For solving the set of partial differential-algebraic equations, Eqs. (5)–(9), the spatial variable z is discretized by taking 150 intervals, and the spatial derivatives are approximated by a second-order backward finite difference scheme. In this way, the original system becomes reduced to a system of ordinary differential–algebraic equations (DAEs) in the time variable. The backward approximation enables that the DAEs at any axial position z do not depend on the values of upwards variables. This feature permits a successive temporal solution from the first up to the final spatial node (at $z=L$). In each step, conventional routines of solution for DAEs are employed. The true evolution from initial conditions until the CSS can be evaluated in this way. However, as only the definition of the CSS is desired here, an algorithm for accelerating the convergence to the CSS, based on the results at the end of successive semicycles, has been employed and described by Luzi (2015).

3.2. Boundary and initial conditions for the RRFR and solution for the CSS

Under the assumptions discussed in Section 3, it can be concluded that each channel of the RRFR will show the same behaviour once the CSS is reached. However, at variance with the CRFR, the evolution of temperatures and concentrations in the channels from certain initial conditions (even when these conditions were the same for all channels) will follow different paths. This is because when the operation starts (by rotating the bed and allowing the incoming of the prescribed flow of VOC laden air), the channels in each compartment will reach the next one at different times, according to the initial angle α_0 that separates the channels from the compartment boundary, $t_{\alpha 0}=\alpha_0\, t_{cycle}/(2\pi)$. Then, channels with different values of $t_{\alpha 0}$ will start their journey in the new compartment with different temperature and concentration profiles. This initial distinction will progressively fade away, as the CSS is approached. Therefore, as we are just interested in the CSS, the evolution of a single channel initially just at the beginning of a reaction compartment, $\alpha_0=(1-f_C)\pi$, will be evaluated. Yet, an approximation has to be made to compute the evolution of the test channel. When it enters in the cleaning compartment, a stream of temperature and composition $\langle T_G\rangle^R$ and $\left\langle y_{j,G}\right\rangle^R$ feeds the channel. In general, $\langle T_G\rangle^R$ and $\left\langle y_{j,G}\right\rangle^R$ are the result of mixing the discharges of all channels in the reaction compartment. In the CSS, these values are independent of time, but during the actual evolution they will be time-dependent and, furthermore, they will depend of the evolution of all channels. Therefore, as we only follows the evolution of the test channel, the value of $\langle T_G\rangle^R$ and $\left\langle y_{j,G}\right\rangle^R$ are estimated from averaging the temperature and concentration of the discharge of the test channel in its journey from the previous reaction compartment. Thus, denoting τ the time at which the channel just reaches the cleaning compartment (Fig. 3), the following expressions allow evaluating $\langle T_G\rangle^R$ and $\left\langle y_{j,G}\right\rangle^R$:

$$\left\langle y_{j,G}\right\rangle^R = \frac{1}{t_R}\int_{\tau-t_R}^{\tau} y_{j,G}(t,L)\; dt, \tag{11}$$

$$t_R\int_{T_0}^{\langle T_G\rangle^R} c_{pG}(T)dT = \int_{\tau-t_R}^{\tau}\left[\int_{T_0}^{T_G(t,L)} c_{pG}(T)dT\right]dt, \tag{12}$$

where t_R is given in Eq. (3). The values of $\langle T_G\rangle^R$ and $\left\langle y_{j,G}\right\rangle^R$ are kept constant during the journey of the test channel in the cleaning compartment, $\tau<t<\tau+t_C$ (see Eq. (4) for t_C).

As Eqs. (11) and (12) do provide the correct values of $\langle T_G\rangle^R$ and $\left\langle y_{j,G}\right\rangle^R$ at the CSS, the evolution of the test channel will be approximated, but the CSS will be correctly evaluated.

Initial conditions for the test channel are taken just as for the CRFR, i.e. $y_{j,G}(0,z)=0$ (clean air), $T_S(0,z)=T_G(0,z)=T^{ini}=350$ °C. Besides, Eq. (10) is employed when the test channel just leaves a cleaning compartment and enters in the next reaction compartment, i.e. when flow reversal occurs, and the acceleration procedure (Luzi, 2015) is also applied. Thus, apart from the inclusion of the cleaning steps, calculations follow much in the same way as for the CRFR.

A final comment deserves the choice of the flow rate of the cleaning streams. They should guarantee the complete displacement of the volume of air contaminated with VOCs in the inlet zone after the cleaning time t_C. The criterion adopted to fix such a flow rate is presented in the Appendix.

4. Preliminary analysis of the reverse-flow systems

Before establishing a design criterion, it is convenient to accomplish an analysis of the behaviour of the system upon varying the most significant operatives and design parameters. The diameter/length ratio of the bed is excluded from the analysis, as this ratio will only influence the total pressure drop.

Fig. 4 shows the response to a variation in cycle period, t_{cycle}, for the CFCR employing the cell configuration #4 (Table 3). The VOC content corresponds to the minimum value considered (Table 1), and different values are employed for the total length of the unit and for the ratio f_I between the length of the inert zones and the total length (*inert fraction*, for short). The variables chosen to represent the behaviour of the system are the maximum

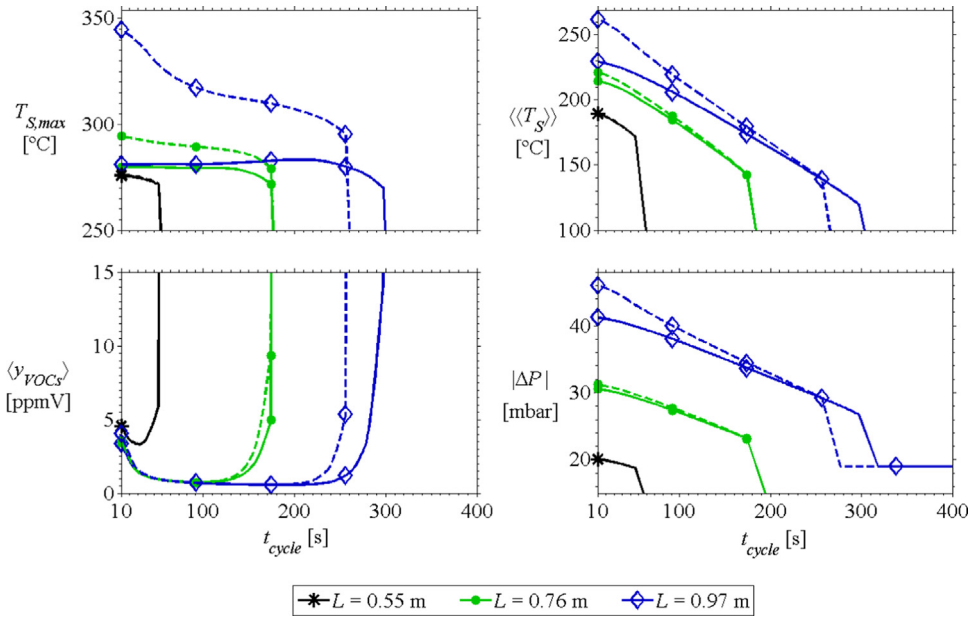

Fig. 4. Impact of the cycle period on the CRFR at the minimum inlet VOCs concentration (Table 3) for different values of the total length, L, and the inert fraction, f_I. The solid and dashed lines correspond to f_I = 30% and f_I = 50%, respectively. D=2.2 m, G=3.35 kg/(m^2 s), Re=255.

temperature of the solid material, $T_{S,max}$, the average temperature of the solid material during a semicycle, $\langle\langle T_S \rangle\rangle$, the average global emission of VOCs, $\langle y_{VOCs} \rangle$, and the total pressure drop, $|\Delta P|$. For the CSS, $\langle\langle T_S \rangle\rangle$ is calculated according to:

$$\langle\langle T_S \rangle\rangle = \frac{1}{(t_{cycle}/2)\ L} \int_0^{t_{cycle}/2} \int_0^L T_S \ dz \ dt \tag{13}$$

where the time was zeroed at the beginning of the semicycle.

As t_{cycle} increases, for a given set of parameters, a value $t_{cycle,crit}$ is reached at which $\langle y_{VOCs} \rangle$ suddenly increases, i.e. the reaction extinguishes. Fig. 4 reveals that $t_{cycle,crit}$ increases with L. This result, previously pointed out by Cittadini et al. (2001), can be explained by recalling that the thermal wave formed during the CSS will travel at a roughly constant velocity. As long as the wave front does not leave the catalytic region, the ignited CSS will be maintained. Clearly, larger beds will allow operating at higher t_{cycle} without extinction.

For high values of L (*i.e.*, L=0.97 m in Fig. 4) a strong dependence of $T_{S,max}$ on the inert fraction f_I is observed, a feature discussed by Matros et al. (1993). For a small value of f_I (*i.e.*, 30% in Fig. 4), $T_{S,max}$ becomes practically insensitive to the cycle period used, as long as t_{cycle} is not very close to $t_{cycle,crit}$. On the contrary, for f_I=50%, $T_{S,max}$ decreases monotonically as t_{cycle} increases. In order to explain this difference, we first consider the case when f_I=0 and analyse what happens as t_{cycle} is increased. Starting from a very short value of t_{cycle}, just above the gas residence time, it should be realized that the temperature profile will be nearly stationary and symmetric (the limiting stationary profile corresponds to the operation of a hypothetical countercurrent reactor, as noted by Eigenberger and Nieken (1994)). From any of the ends, the temperature steadily increases up to a distance L_{ign} at which

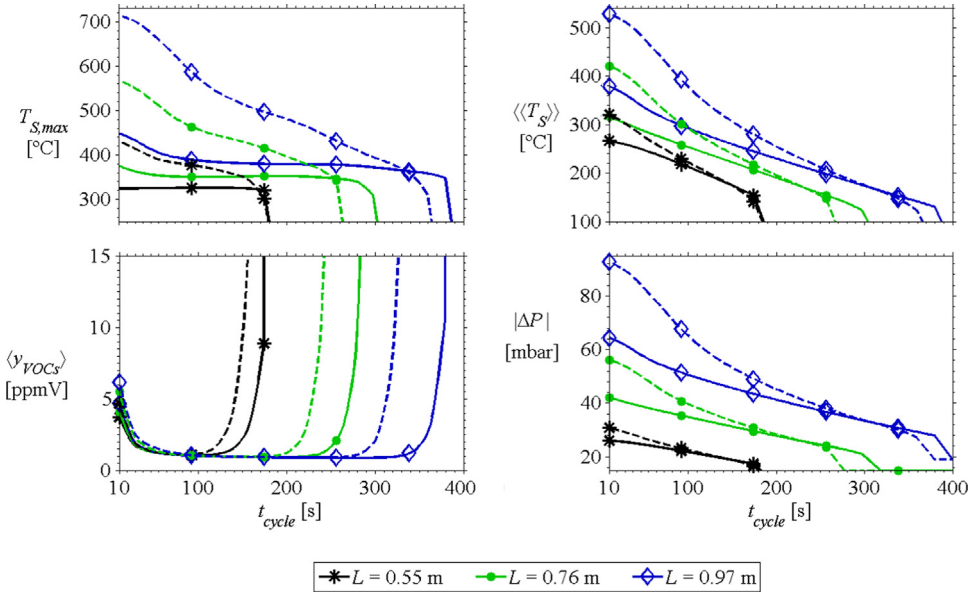

Fig. 5. Impact of the cycle period on the CRFR at the nominal inlet VOC concentration (Table 3) for different values of the total length, L, and the inert fraction, f_I. The solid and dashed lines correspond to f_I = 30% and f_I = 50%, respectively. D=2.2 m, G=3.35 kg/(m^2 s), Re=255.

the ignition temperature T_{ign} is reached, *i.e.* a temperature ramp can be identified between $0 < z < L_{ign}$. Further inside the bed, the combustion reactions already take place and the temperature remains nearly constant over a central plateau of length $L_p = L - 2L_{ign}$. The maximum temperature on the plateau is around $T_{S,max} = (T_{ign} + \Delta T_{ad})$, a value that also characterizes the overall plateau temperature (Eigenberger et al., 2007). At a higher enough value of t_{cycle}, the temperature profile will be no longer stationary nor symmetric at any time during each semicycle. During most part of a semicycle, approximately the same temperature ramp can again be identified close to the input end, but it moves leaving behind a cold zone from $z=0$, at nearly the inlet temperature. The maximum length reached by the cold zone increases with t_{cycle} at the expense of the plateau length, which maintains the temperature level approximately defined by $T_{S,max} = (T_{ign} + \Delta T_{ad})$. At the conditions of Fig. 4, L_{ign} is similar to the product $L_I = (f_I/2)L$ when $f_I = 30\%$ and $L = 0.97$ m; therefore the behaviour in this case is quite similar to that just described for $f_I = 0$. The small increase of $T_{S,max}$ shown in Fig. 4 in the lower range of t_{cycle} is owing to the development and stabilization of the wave front. The final decrease and, ultimately, the sudden drop of $T_{S,max}$ take place when L_p becomes strongly reduced, *i.e.* when the plateau is about to disappear and the reaction about to become extinguished. On the other hand, for $f_I = 50\%$ and $L = 0.97$ m, $L_I = (f_I/2)L$ exceeds significantly the value L_{ign}. At a very low t_{cycle}, again a nearly stationary and symmetric profile develops, but the temperature ramp now extends along the whole length L_I, and consequently a higher value $T_{S,max} > (T_{ign} + \Delta T_{ad})$ is reached at the point the catalytic central zone begins (Fig. 4). At a high value of t_{cycle}, the length L_I is partially covered by the cold zone, the ramp is shorten and therefore $T_{S,max}$ decreases. The longer t_{cycle}, the lower $T_{S,max}$, as the cold zone becomes larger (Fig. 4).

In addition, independently of the inert fraction or the total length of the unit, the average temperature of the solid material in the bed, $\langle\langle T_S \rangle\rangle$ always diminishes with an increase in t_{cycle}. This effect is due to the broadening of the cold zone. This shows that $\langle\langle T_S \rangle\rangle$ is a good indicator of the temperature regime of the reactor, when used as a complement of the typical parameter $T_{S,max}$. On the other hand, as expected, low values of $\langle\langle T_S \rangle\rangle$ bring as a consequence a decrease in the pressure drop, as a result of a lower kinematic viscosity.

The average emission of VOCs $\langle y_{VOCs} \rangle$ shows a minimum with t_{cycle} before $t_{cycle,crit}$ is reached. Exception made for the shortest bed, $L = 0.55$ m, the minimum is about 1 ppmV. The rise when $t_{cycle,crit}$ is approached is clearly due to sudden drop of $T_{S,max}$, and the rise as $t_{cycle} \to 0$ is due to the already discussed wash-out problem.

Fig. 5 shows the results of the same analysis, but for an operation with the nominal VOC concentrations. First, the response is qualitatively similar. Nevertheless, because of the greater content of VOCs in the air stream to be treated, the average value $\langle\langle T_S \rangle\rangle$ is significantly higher than in Fig. 4, and consequently the pressure drop increases. It should be emphasized that for given values of L and t_{cycle}, the differences in behaviour for the different values of the inert fraction f_I become substantially more pronounced than in the case with a lower content of VOCs, owing to the greater driving force for the heat exchange (*i.e.*, a greater ΔT_{ad}). This feature will be shown to be significant in Section 5 because they limit the value of f_I when a restriction in the maximum temperature of the solid material is imposed.

It is also noted that in all situations the value of $t_{cycle,crit}$ is higher than the corresponding value for the operative condition with the minimum VOC content, and becomes more sensitive to variations in f_I, especially when L is large.

The average VOC emission exhibits a behaviour completely similar in both, Figs. 4 and 5, including the lowest emission level achievable (*ca.* 1 ppm V).

Fig. 6 presents a comparison between the responses of the two systems, CRFR and RRFR, for the operation with the nominal VOC content, for the values of L considered previously, an inert fraction of 50%, and a cleaning fraction of 2% in the RRFR. As expected, the thermal behaviour of both systems is equivalent (with the largest difference in $T_{S,max}$ being about 12 °C). Furthermore, the pressure drop in the RRFR is slightly higher, as a consequence of the presence of the cleaning step, reaching values up to 30% higher than those in the CRFR. The greatest differences are observed at low cycle periods since the mass flow rate used in the cleaning step is inversely proportional to t_{cycle} (see Eq. (A.1) in the Appendix).

It should be noted that $\langle y_{VOCs} \rangle$ in the RRFR reached values that are practically nil for low values of t_{cycle}, due to the cleaning step. Moreover, this also reveals that $\langle y_{VOCs} \rangle$ in the CRFR at short cycle periods is completely dominated by the wash-out problem.

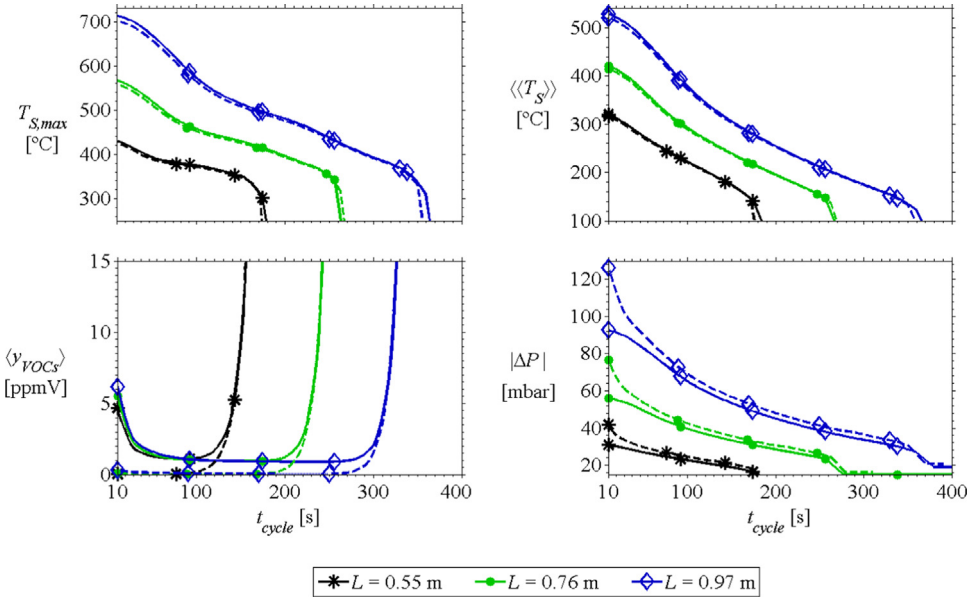

Fig. 6. Comparison between the CRFR and RRFR operations at the nominal inlet VOCs concentration for different values of L. The solid and dashed lines correspond to the CRFR and RRFR, respectively. $D = 2.2$ m, $f_I = 50\%$. CRFR: $G = 3.35$ kg/(m^2 s), $Re = 255$. RRFR: $G = 3.41$ kg/(m^2 s), $Re = 260$, $f_C = 2\%$.

5. Design procedure and analysis of the results

Having defined a cell configuration, four degrees of freedom for the CRFR (f_I, L, D, and t_{cycle}) and five for the RRFR (the previous four plus the cleaning fraction, f_C) can be identified. The cleaning fraction f_C is not a critical parameter. It has been checked that choosing $f_C = 2\%$ avoids the emission of residual VOCs without excessively increasing the pressure drop or reducing the thermal level of the bed, as has been discussed in more detail by Luzi (2015).

Among these degrees of freedom, t_{cycle} – the only operating variable – could take different values for the operations with nominal and minimum VOC contents. In addition, once the unit is installed, t_{cycle} is typically the most relevant (and often the single) control variable. In order to saturate the available degrees of freedom, several restrictions will be imposed.

Being fixed the flow rate of the waste air stream, it is assumed that a blower has been chosen and consequently the maximum pressure drop through the reactor, $|\Delta P|^{adm}$, is also determined. A value $|\Delta P|^{adm} = 50$ mbar, has been employed in this study. Then, the first criterion assumed is that the operation at the nominal VOC content – the situation leading to the higher pressure drop (Figs. 4 and 5) – is carried out accomplishing $|\Delta P| \approx |\Delta P|^{adm}$. As the diameter D is the most relevant variable in determining $|\Delta P|$, the criterion leads to the lowest possible value of D. This is the desired effect in consideration of better flow distribution and minimum cost of the reactor heads.

The second restriction concerns the limit in the emission of VOCs. According to the regulations established by the European Commission (Directive 2010/75, 2010), and considering the type of VOCs and the type of activity that generates them, the maximum VOC concentration allowed is 20 mgC/Nm^3, which represents a VOC content between 9 and 20 ppm V – depending on the ratio of the ethyl acetate to the ethanol in the discharge –. Nonetheless,

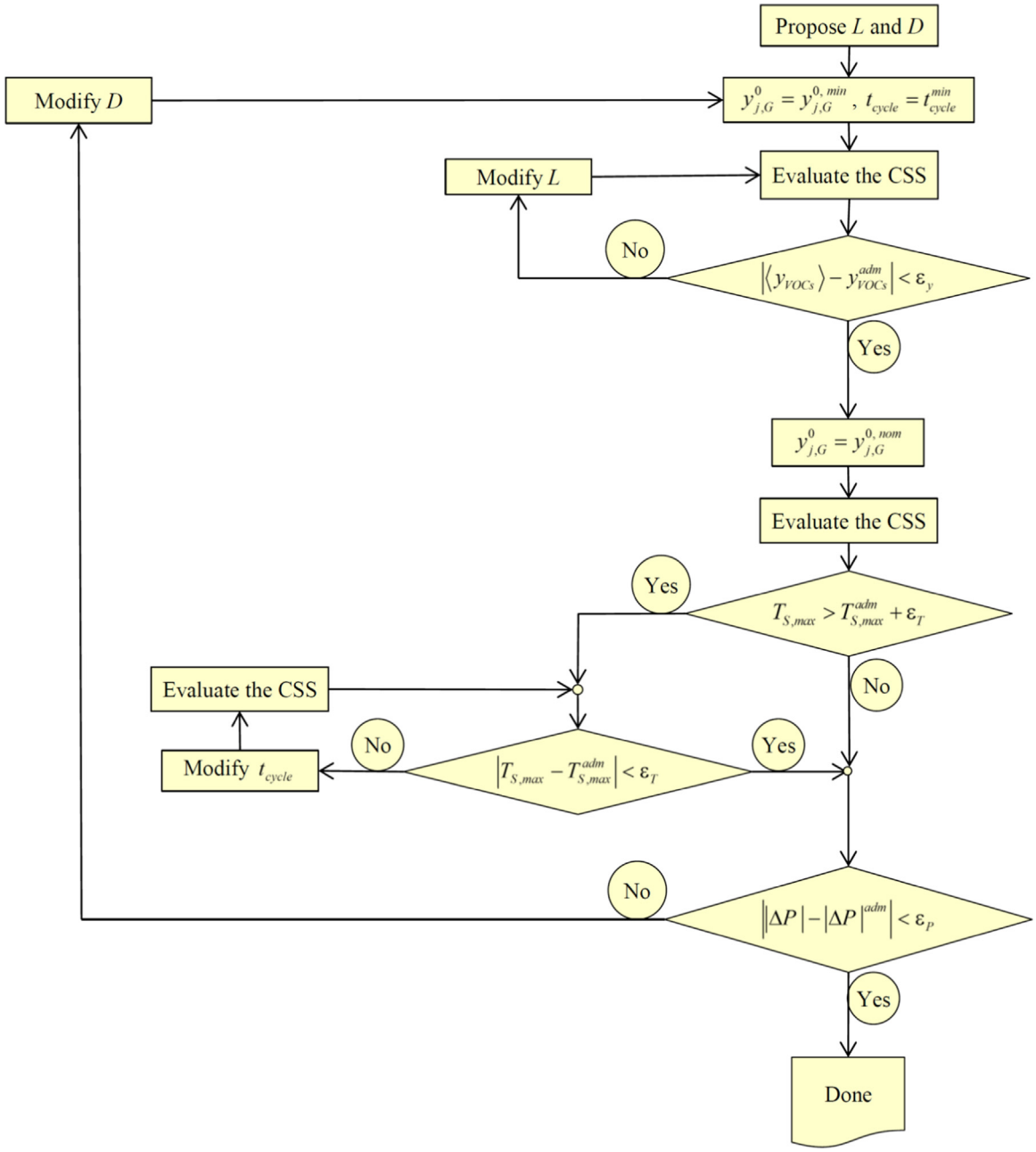

Fig. 7. Flowchart of the design strategy proposed.

that value is not adequate as a maximum tolerable emission for consideration as a design restriction since that concentration is found in the region close to the extinction of the reactor (see Figs. 4 and 5). Therefore, as a practical restriction for the VOC content at the reactor outlet, a value $y_{VOCs}^{adm}=1$ ppmV has been established. Furthermore, as was discussed in Section 4, the values of $t_{cycle,crit}$ for a given L are substantially lower for the operating condition involving the minimum VOC content than for the nominal level. Consequently, the operating condition at the minimum VOC content should be chosen to fulfil the condition $y_{VOCs}^{adm}=1$ ppm V. Regarding the logic of the design strategy, this requirement is associated with the setting of the reactor length L.

High temperature levels can be achieved from the reverse flow operation and this feature is desirable for a design with a low catalyst loading. However, the maximum temperature level tolerated by the catalytic material should be considered in any practical design. For the catalyst under consideration, no data are available on its thermal stability. It was therefore taken as a conservative value – in consideration of an oxide mixture as catalytic material – a maximum allowable temperature of 400 °C, assumed to represent a level from which catalyst deactivation is strongly enhanced. Temperature is then subject to the inequality restriction $T_{S,max} \le T_{S,max}^{adm}$. As short cycle period allows operating at high temperatures (Section 4), t_{cycle} is the variable associated in the design strategy to control the temperature level. In turn, the own operating value t_{cycle} has been restrained in accounts of practical recommendations. A minimum value $t_{cycle}^{min}=240$ s was adopted for the CRFR scheme, which implies a valve lifetime of at least 2 years according to Barresi et al. (2007). For the RRFR scheme, the maximum rotational speed is restrained to 2 rpm, according to the lower limit of the usual range of rotary heat exchangers, and therefore $t_{cycle}^{min}=30$ s. In short, for the operation with either nominal or minimum VOC content, the minimum value of t_{cycle} subject simultaneously to $t_{cycle} \ge t_{cycle}^{min}$ and $T_{S,max} \le T_{S,max}^{adm}$ is retained in the design strategy.

As regards the inert fraction f_I, a convenient minimum value will be such that $L_I=(f_I/2)L=L_{ign}$ at the minimum VOC content (L_{ign} is larger) to replace an equivalent length of unused catalytic material (see discussion in Section 4). Longer values of L_I will allow saving further amounts of catalyst, but at a very moderate rate. To find out the optimal value of L_I or f_I, it will be necessary to carry out a formal optimization involving the unitary costs of inert and catalytic materials. However, a fruitful optimization based on economic grounds will have to include all aspects involved in the unit design, catalyst deactivation rates for evaluating its useful life, and operating costs, such as that for compression. Therefore, to keep the comparison between the CRFR and RRFR alternatives on simple and conceptual bases, the fraction f_I has been fixed in 40% and 50% for the CRFR and RRFR, respectively. These values ensure that $L_I > L_{ign}$ at minimum VOC contents. Besides, the lower fraction f_I for the CRFR was chosen to avoid an excessive length L_I, as higher values of the catalytic length are needed on account of longer t_{cycle}^{min} (see Section 4).

A flowchart showing the sequence for the design described here is given in Fig. 7. The minimum and nominal VOC contents in the air stream to be treated are identified as $y_{j,G}^{0,min}$ and $y_{j,G}^{0,nom}$, respectively. In addition, ε_y, ε_T and ε_P are the tolerances adopted for the emission level (0.01 ppm V), maximum bed temperature (5 °C), and pressure drop (1.5 mbar), respectively. It must be emphasized that for the steps in Fig. 7 involving the operating conditions at the minimum VOC content $t_{cycle}=t_{cycle}^{min}$ was always found to be feasible. Thus, for simplicity, the restrictions $t_{cycle} \ge t_{cycle}^{min}$ and $T_{S,max} \le T_{S,max}^{adm}$ were not included in Fig. 7.

It should be stressed that the proposed design strategy turned out to be feasible for both, CRFR and RRFR, and for all cell configurations defined in Table 3. However, the same result cannot be guaranteed for different systems (as defined by the characteristics of the VOC laden stream, type of catalyst and reactor configuration) and/or different settings for the set of parameters defining the restrictions $|\Delta P|^{adm}$, $\langle y_{VOCs}^{adm} \rangle$, t_{cycle}^{min}, $T_{S,max}^{adm}$.

The results for the CRFR and each of the cell configurations given in Table 3 are summarized in Table 4. W_I and W_{cat} are the total mass of the inert and catalytic materials, respectively, which are calculated according to:

$$W_I = \rho_I \, V\left[f_I(1-\varepsilon) + (1-f_I)(1-\varepsilon - a_v \ell)\right] \tag{13}$$

$$W_{cat} = \rho_{cat} \, V(1-f_I) a_v \ell \tag{14}$$

Based on the values of W_I and W_{cat}, configurations #3 and #5 appear to be good alternatives. Nevertheless, these designs operate under conditions very close to the extinction of the reactor, as is reflected in the relationship $(t_{cycle,crit} - t_{cycle})/t_{cycle}$ for the nominal

Table 4
Resulting dimensions for the CRFR for each monolith cell described in Table 3.

	Cell configuration	#1 (200/12.5)	#2 (400/7.5)	#3 (600/4)	#4 (400/8.8)	#5 (600/7.2)
	V [m^3]	5.12	3.66	4.34	3.39	2.86
	L [m]	1.61	1.14	1.21	0.996	0.802
	D [m]	2.01	2.02	2.14	2.08	2.13
	W_I [kg]	4001	2401	1801	2606	2174
	W_{cat} [kg]	156	163	251	146	151
	G [kg/(m^2 s)]	4.01	3.97	3.54	3.74	3.57
	Re	446	302	207	294	229
Minimum inlet VOC concentration	$T_{S,max}$ [°C]	273	289	321	285	302
	$\langle y_{VOCs} \rangle$ [ppm]	0.992	0.999	1.01	0.998	1.00
	$\lvert\Delta P\rvert$ [mbar]	37.1	42.1	44.6	40.0	44.4
Nominal inlet VOC concentration	t_{cycle} [s]	240	276	272	270	284
	$t_{cycle,\ crit}$ [s]	581	378	323	400	348
	$(t_{cycle,\ crit}/t_{cycle})-1$	1.42	0.37	0.19	0.48	0.23
	$T_{S,max}$ [°C]	371	398	400	399	396
	$\langle y_{VOCs} \rangle$ [ppm]	0.777	0.875	1.50	0.708	0.848
	$\lvert\Delta P\rvert$ [mbar]	49.4	49.8	48.9	48.9	49.8

Table 5
Comparison between selected design for the CRFR and RRFR.

	Scheme Cell configuration	CRFR #4 (400/8.8)	RRFR #5 (600/7.2)
	V [m^3]	3.39	1.54
	L [m]	0.996	0.49
	D [m]	2.08	2.01
	W_I [kg]	2606	1183
	W_{cat} [kg]	146	68
	G [kg/(m^2 s)]	3.74	4.01
	Re	294	257
Minimum inlet VOC concentration	$T_{S,max}$ [°C]	285	282
	$\langle y_{VOCs} \rangle$ [ppm]	0.998	1.00
	$\lvert\Delta P\rvert$ [mbar]	40.0	42.9
	$G_{m,C}/G_{m,tot}$ [‰]	–	3.16
Nominal inlet VOC concentration	t_{cycle} [s]	270	66
	$t_{cycle,\ crit}$ [s]	400	152
	$(t_{cycle,\ crit}/t_{cycle})-1$	0.48	1.30
	$T_{S,max}$ [°C]	399	398
	$\langle y_{VOCs} \rangle$ [ppm]	0.708	0.009
	$\lvert\Delta P\rvert$ [mbar]	48.9	49.4
	$G_{m,C}/G_{m,tot}$ [‰]	–	1.11

VOC content. For this reason, the use of such configurations for the CRFR is not recommended. As to the remainder, the design with the cell configuration #1 is the one that presents the largest ratio $(t_{cycle,crit} - t_{cycle})/t_{cycle}$, but also is the one requiring the largest values of W_I and W_{cat}. Finally, the designs with the cell configurations #2 and #4 need intermediate values of W_I and W_{cat}. In addition, the design with configuration #4 involves a somewhat lower W_{cat} and a higher ratio $(t_{cycle,crit} - t_{cycle})/t_{cycle}$ than configuration #2. Therefore, for the CRFR scheme, the cell configuration #4 was selected as being the most satisfactory design.

Following a similar analysis on the results for the RRFR with the five cell configurations listed in Table 3, the design with cell configuration #5 turned out to be the most adequate (details are given in Luzi, 2015). It should be noted that for all the cell configurations the average VOC emission for the nominal operating condition is very much lower than the limits established by the norms of the European Commission mentioned above and in fact reaches practically null values.

Table 5 summarizes the results for the chosen configurations of the RRFR (configuration #5) and CRFR (configuration #4). Because of the lower t_{cycle}^{min}, the RRFR proves to be substantially more compact. Indeed, the selected design of the RRFR require 55% less inert and 53% less catalytic material than the corresponding design of the CRFR, a feature that presumably would have a strong impact on the cost of the unit. In addition, the presence of the cleaning stage in the RRFR does not have a marked influence on the diameter required, which in fact attains a value quite similar to that found in the CRFR.

The lower quantity of material required in the RRFR leads to a reduction in the critical cycle periods $t_{cycle,crit}$ for the nominal VOC content in comparison with the CRFR. Nonetheless, to face uncertainties in the design procedure or variations in the characteristics of the air-stream, the relevant magnitude is the difference $\Delta t_{oper} = t_{cycle,crit} - t_{cycle}$, which is similar for both types of reactors. Besides, the relative difference $\Delta t_{oper}/t_{cycle}$ is significantly greater for the RRFR. This is another point in favour of the RRFR, as a large value will facilitate the control of the unit.

Another interesting additional aspect with respect to the differences between the two schemes arises from a comparison of the results for each type of cell configuration individually. Thus, for the same type of cell configuration, the requirement for inert and catalytic material in the CRFR is always greater than in the RRFR, as a consequence of a higher value of t_{cycle}^{min}. For the cells analysed here, such differences lie between 20% and 62% for the inert and between 34% and 69% for the catalytic material. The higher values correspond to the designs with the cell configuration #3, which shows the largest void fraction (see Table 3), and therefore enables the thermal wave front to move at a higher velocity, thus increasing the influence of t_{cycle}^{min} on the dimensions of the unit.

The results of the present study suggest that the rotatory scheme is more convenient than the conventional one. The significant difference in size is largely due to the lower value of t_{cycle}^{min} for the RRFR. Revealing the impact of this variable is regarded as a valuable outcome of this study. However, it should be borne in mind that the values of t_{cycle}^{min} have been adopted from literature recommendations, but in practice information should be gathered from potential suppliers of the devices for flow reversal (either the valve or rotation systems). Eventually, if the effect of t_{cycle} on the maintenance cost of such devices is made available, an analysis based on economic grounds can disclose the convenience for shortening t_{cycle}. Yet, the wash-out problem will still remain for the CRFR and impose a natural limitation. In this regard, it is noted that for the case here studied, the emission of VOCs begins to increase for values of t_{cycle} lower than *ca.* 50 s.

6. Conclusions

Two reverse-flow systems were analysed for the treatment of an air stream contaminated with ethyl acetate and ethanol: a conventional scheme operated with a valve system for flow reversal (CRFR) and one employing the rotation of the catalytic bed (RRFR) for the same purpose. A monolithic structure with square channels was assumed for both types of reverse-flow reactors. Under the assumption that the angular thermal conduction is negligible in the RRFR, a single model was utilized to simulate the operation of both alternatives. The inclusion of a cleaning step was considered in the RRFR. With this model, the response of both systems was studied upon modifying variables such as the VOC content in the air stream to be treated, the total length of the unit, the inert fraction, and the cycle period. A comparison of the individual responses of the two schemes under identical conditions demonstrated that the inclusion of a cleaning fraction of 2% of the RRFR total volume avoids the emission of unreacted VOCs in the entrance region of the unit when the flow reversal is performed, without affecting the overall performance of the system.

A design strategy was proposed taking into account that the VOC content can decrease down to half of the nominal level. Based on that strategy, the dimensions for both reverse-flow schemes were sought, considering 5 different cell configurations of the monolithic structure. For each of the two schemes, the most adequate cell configuration was selected upon consideration of the quantity of inert and catalytic material required and the feasible range of cycle periods in the nominal operating condition.

Although both systems proved to be adequate, the RRFR exhibits clear advantages. This scheme requires 55% less inert and 53% less catalytic material. Such a difference leads to a reduction in the critical cycle period for the nominal operating condition, but the range of cycle periods relative to the value selected in the design is significantly greater.

Nomenclature

a_v	specific interfacial area (m^{-1})
c_p	specific heat ($J\,kg^{-1}\,K^{-1}$)
C_T	total molar concentration in the gas phase ($mol\,m^{-3}$)
D	diameter of the unit (m)
d_h	hydraulic diameter of the channels (m) ($4\varepsilon_L/a_v$)
E_i	activation energy of the ith reaction ($J\,mol^{-1}\,K^{-1}$)
f_C	cleaning fraction (RRFR)
f_I	inert fraction
G	superficial mass velocity ($kg\,m^{-2}\,s^{-1}$)
$G_{m,C}$	cleaning mass flow rate (RRFR) ($kg\,s^{-1}$)
$G_{m,C,min}$	minimum cleaning mass flow rate (RRFR) ($kg\,s^{-1}$)
$G_{m,tot}$	total mass flow rate to be treated ($kg\,s^{-1}$)
h	heat transfer coefficient ($W\,m^{-2}\,K^{-1}$)
h^*	modified heat transfer coefficient (Eq. (6)) ($W\,m^{-2}\,K^{-1}$)
k_i	specific rate constant of the ith reaction (s^{-1})
$k_{i,ref}$	specific rate constant of the ith reaction, evaluated at T_{ref} (s^{-1})
K_j	adsorption constant of the jth component ($m^3\,mol^{-1}$)
$k_{m,j}$	mass transfer coefficient for the jth component ($m\,s^{-1}$)
ℓ	equivalent washcoat thickness (m)
L	length of the unit (m)
L_{cell}	side of the unit cell of the monolith (m)
L_{ign}	minimum length needed to reach the ignition temperature (m)
L_P	length of the central plateau (m)

M_{air} molecular weight of air
n current semicycle to be simulated
N_{cell} number of cells per unit of cross-sectional area (m^{-2})
Nu Nusselt number
r_i ith reaction rate (mol m^{-3} s^{-1})
r_j^{ef} effective rate of consumption of the jth component (mol m^{-3} s^{-1})
R ideal gas constant (J mol^{-1} K^{-1})
Re Reynolds number (evaluated at feed conditions)
Sh Sherwood number
$\langle T_G \rangle^R$ average temperature of the air stream at the output of the reaction step (RRFR) (K)
$\langle\langle T_S \rangle\rangle$ average temperature of the solid material during a semicycle (K)
t time (s)
$t_{\alpha 0}$ time at which a channel in the position α_0 at initial time (in the reaction compartment), reaches the cleaning compartment for the first time
t_{cycle} cycle period (s)
t_{cycle}^{min} minimum cycle period (s)
$t_{cycle,crit}$ critical cycle period (s)
t_C duration of the cleaning stage (RRFR) (s)
t_R duration of the reaction stage (RRFR) (s)
T temperature (K)
T_{ign} ignition temperature of the VOC mixture (K)
T_{ref} reference temperature for the calculation of the kinetic coefficients (K)
$T_{S,max}$ maximum temperature reached in the solid phase (K)
$T_{S,max}^{adm}$ maximum allowable temperature in the solid phase used in the design (K)
V total volume of the unit (m^3)
W_{cat} total mass of the catalytic material (kg)
W_I total mass of the inert material (kg)
$X^{(n)}$ any of the variables T_S, T_G or $y_{j,G}$ for the nth semicycle
$\langle y_{j,G} \rangle^R$ average mole fraction of the jth component in the gas phase at the output of the reaction step (RRFR)
$\langle y_{VOCs} \rangle$ average mole fraction of VOCs at the output
$y_{j,G}^{0,min}$ minimum VOC content
$y_{j,G}^{0,nom}$ nominal VOC content
y_{VOCs}^{adm} allowable mole fraction of VOCs
y_j mole fraction of the jth component
z axial position in the channel (m)

Greek letters

α_0 initial angle formed by a series of channels aligned on the radius of the rotor, measured from the separation between the reaction and cleaning compartments (RRFR)
ΔH_j enthalpy of combustion of the jth component (J mol^{-1})
Δt_{oper} difference between $t_{cycle,crit}$ and t_{cycle} (s)
ΔT_{ad} maximum adiabatic temperature rise (K)
δ_{cat} catalytic coating thickness (m)
δ_T wall thickness (m)
ε void fraction of the bed
ε_P tolerance for the pressure drop (1.5 mbar)
ε_T tolerance for the maximum temperature (5 K)
ε_y tolerance for the total VOC emission (0.01 ppm V)
λ thermal conductivity (W m^{-1} K^{-1})
$|\Delta P|^{adm}$ allowable pressure drop (absolute value) (mbar)
$|\Delta P|$ pressure drop in a cycle (mbar)
ρ density (kg m^{-3}).
τ time at which the channel just reaches the cleaning compartment (RRFR).

Subscripts

cat catalyst-associated property or variable
C cleaning step
G gas-phase-associated property or variable
i ith reaction
I property or variable associated with the inert region of the units
S property or variable associated with the solid phase or the interfacial area between the gas and solid phases

Superscripts

0 feed conditions
ini initial condition

Acknowledgements

The authors wish to thank the financial support of the following Argentine institutions: ANPCyT-MINCyT (PICT'11 – 1641), CONICET (PIP 0304), and UNLP (PID 11/I177). O. M. Martínez and G. F. Barreto are Research Members of CONICET.

Appendix. Determination of the cleaning flow rate

It should be born in mind that the use of high flow rates should be avoided since such an option would only contribute to increase the pressure drop and cool the solid material. For the purpose of the present analysis, the minimum mass flow rate used in the cleaning step could be estimated by considering that the total volume containing VOCs in the entrance portion of the channels must be displaced up to the hot region of the catalyst by the end of the cleaning step. Once the cleaning fraction f_C has been defined, the minimum mass flow rate $G_{m,C,min}$ can be estimated under the assumption that the temperature profile in the gas stream remains unaltered during the cleaning step. Then,

$$G_{m,C,min} = \frac{\varepsilon f_C \; S_{tot}/2}{t_C} \quad \int_0^{z^\#} \rho_G \; dz \tag{A.1}$$

where S_{tot} is the total cross section and $z^\#$ the position in which the total conversion of VOCs has reached 99% at the end of the reaction step (or $z^\# = L$ if the total conversion is less than that figure). t_C is related to t_{cycle} through Eq. (4) ($f_C/t_C = 2/t_{cycle}$) and the gas density, ρ_G, must be evaluated at $T_G(\tau, z)$, where τ is the time at which the channel just reaches the cleaning compartment.

Finally, introducing a security factor, the mass flow rate used in the cleaning step is taken as:

$$G_{m,C} = 1.1 \; G_{m,C,min} \tag{A.2}$$

References

Barresi, A.A., Baldi, G., Fissore, D., 2007. Forced unsteady-state reactors as efficient devices for integrated processes: case histories and new perspectives. Ind. Eng. Chem. Res. 46 (25), 8693–8700.
Boger, T., Heibel, A., Sorensen, C.M., 2004. Monolithic catalysts for the chemical industry. Ind. Eng. Chem. Res. 43 (16), 4602–4611.
Campesi, A., Luzi, C.D., Martínez, O.M., Barreto, G., 2012a. Effect of concentration by thermal swing adsorption on the catalytic incineration of VOCs. Int. J. Chem. React. Eng. 10 (1), A54.

Campesi, M.A., Mariani, N.J., Bressa, S.P., Pramparo, M.C., Barbero, B.P., Cadús, L.E., Barreto, G.F., Martinez, O.M., 2012b. Kinetic study of the combustion of ethanol and ethyl acetate mixtures over a MnCu catalyst. Fuel Process. Technol. 103, 84–90.

Chen, G., Chi, Y., Yan, J., Ni, M., 2011. Effect of periodic variation of the inlet concentration on the performance of reverse flow reactors. Ind. Eng. Chem. Res. 50 (9), 5448–5458.

Cittadini, M., Vanni, M., Barresi, A.A., Baldi, G., 2001. Simplified procedure for design of catalytic combustors with periodic flow reversal. Chem. Eng. Process. 40 (3), 255–262.

Directive 2010/75/EU of the European Parliament and of the Council, on industrial emissions (integrated pollution prevention and control), 2010. ⟨http://eur-lex.europa.eu/legal-content/ES/TXT/?qid=1422968493087&uri=CELEX:32010L0075⟩, (last accessed in 2015).

Eigenberger, G., Kolios, G., Nieken, U., 2007. Thermal pattern formation and process intensification in chemical reaction engineering. Chem. Eng. Sci. 62 (18–20), 4825–4841.

Eigenberger, G., Nieken, U., 1994. Catalytic cleaning of polluted air: reaction engineering problems and new solutions. Int. Chem. Eng. 34 (1), 4–16.

Gulati, S.T., 2006. Ceramic Catalyst Supports for Gasoline Fuel, Cap. 2 in Structured Catalysts and Reactors. In: Cybulski, A., Moulijn, J.A. (Eds.), 2nd ed. Taylor and Francis, Boca Raton, USA.

Kolaczkowski, S., 2006. Treatment of Volatile Organic Carbon. Emmisions from Stationary Sources: Catalytic Oxidation of the Gaseous Phase, Cap. 5 in Structured Catalysts and Reactors. In: Cybulski, A., Moulijn, J.A. (Eds.), 2nd ed. Taylor and Francis, Boca Raton, USA.

Kolios, G., Frauhammer, J., Eigenberger, G., 2000. Autothermal fixed-bed reactor concepts. Chem. Eng. Sci. 55 (24), 5945–5967.

Lecomte, F., Broutin, P., Lebas, E., 2010. CO2 Capture: Technologies to Reduce Greenhouse Gas Emissions. ed. Technip, Paris, IFP.

Luzi, C.D., 2015. Combustión catalítica de compuestos orgánicos volátiles utilizando sistemas autotérmicos con intercambio de calor regenerativo. Tesis Doctoral, Universidad Nacional de La Plata, Argentina.

Marín, P., Ordóñez, S., Díez, F.V., 2010. Monoliths as suitable catalysts for reverse-flow combustors: modeling and experimental validation. AIChE J. 56 (12), 3162–3173.

Matros, Yu. Sh, Bunimovich, G.A., 1996. Reverse-flow operation in fixed bed catalytic reactors. Catal. Rev. 38 (1), 1–68.

Matros, Yu, Sh., Noskov, Chumachenko, A.S., V. A., 1993. Progress in reverse-process application to catalytic incineration problems. Chem. Eng. Process. 32 (2), 89–98.

Morales, M.R., Barbero, B.P., Cadús, L.E., 2008. Evaluation and characterization of Mn–Cu mixed oxide catalysts for ethanol total oxidation: influence of copper content. Fuel 87 (7), 1177–1186.

Noorman, S., van Sint Annaland, M., Kuipers, J.A.M., 2010. Experimental validation of packed bed chemical-looping combustion. Chem. Eng. Sci. 65, 92–97.

Vortmeyer, D., Schaefer, R.J., 1974. Equivalence of one- and two-phase models for heat transfer processes in packed beds: One dimensional theory. Chem. Eng. Sci. 29, 485–491.

Zhao, Z., Chen, T., Ghoniem, A., 2013. Rotary bed reactor for chemical-looping combustion with carbon capture. Part 1: Reactor design and model development. Energy Fuels 27 (1), 327–343.